Materials International
Open-Access Journal (ISSN: 2668-5728)

Article
Volume 8, Issue 1, 2026, 9
https://doi.org/10.33263/Materials81.009

Wear, Friction Coefficient, and Contact Angle of Sintered Nano Ni-Ti Material Reinforced by Si and Al_2O_3

Mahmoud Farag Zawrah [1,*], Ibrahim Hassab-Allah [2], Hesham Shouib Abdelrahman [2,3,*], Moataz Bellah Hassan Ata [3]

[1] Refractories, Ceramics and Building Materials Department, National Research Centre, 12622 Dokki, Cairo, Egypt
[2] Mechanical Engineering Department, Faculty of Engineering, Assiut University, Assiut, Egypt
[3] Production Department, Faculty of Technology and Education, Sohag University, Sohag, Egyp
* Correspondence: mzawrah@hotmail.com;

Received: 3.12.2024; Accepted: 5.08.2025; Published: 10.03.2026

Abstract: To improve the mechanical properties (friction coefficient and mechanical wear) of sintered Ni-Ti alloy, Si or Al_2O_3 particles (10 wt.%) were added. Before sintering at different temperatures, the nano powders were prepared by mechanical alloying. After milling, the nanocomposite powders were investigated by X-ray diffraction and transmission electron microscopy. The resulting nanocomposite powders were cold-pressed at 500 MPa and sintered for 3 h at 1050, 1100, and 1200°C. The microstructure of sintered samples was examined by scanning electron microscopy. The effect of sintering temperature on tribology and wettability of sintered 50Ni50Ti, 45Ni45Ti10Si, and 45Ni45Ti10Al_2O_3 composites was examined using suitable testing techniques. The results demonstrated that the milled powders are homogeneous in morphology and size. Also, Si and Al_2O_3 reinforcements are uniformly distributed in the NiTi-matrix, and the particle sizes were decreased after milling and reached 21, 27, and 104 nm, for 50Ni50Ti, 45Ni45Ti10Si, and 45Ni45Ti10Al_2O_3 nanocomposites, respectively. The mechanical properties improved with the addition of reinforcements and an increase in the sintering temperature. For the composite 45Ni45Ti10Al_2O_3, the wear rate and friction coefficient were reached 11x10-6mm^3/Nm and 0.17, respectively. Furthermore, the surface energy and wettability of sintered composites were increased with increasing sintering temperature and after the addition of Si or Al_2O_3.

Keywords: Ni-Ti nano material; Si and Al_2O_3 reinforcements; powder metallurgy; sintering; microstructure; mechanical properties.

1. Introduction

Nowadays, metal-matrix composites (MMCs) have received considerable attention due to their excellent properties, such as high hardness, high strength, high elastic modulus, high stiffness, elevated wear resistance, and a low thermal expansion coefficient. Consequently, they can be applied extensively across several industrial applications, including defense, automotive brake rotors, aerospace, spot welding, high-performance switches, electrical contacts, and internal combustion engines [1–3]. Two approaches have been utilized to produce metal-matrix nanocomposites. In the first approach, the reinforcement particles are in situ formed in the matrix through chemical reactions or phase transformations [4–6]. On the other hand, the

second approach relies on the dispersion of reinforcements within the matrix via mechanical blending (in liquid or solid form) or by selectively fracturing secondary particles using mechanical methods [7–9]. Mechanical alloying (MA) is a highly effective technique for synthesizing nanoparticles by repeatedly welding, fracturing, and re-welding powder particles. The starting materials must include at least one ductile metal as a host to retain the other components. During mechanical activation of powders, they weld together and, consequently, new, different composites form. Composite powders are produced totally if the welding and fracturing stages are repeated [10, 11]. Furthermore, MA is useful for preparing composites that are difficult to produce by the traditional melt-cast method [12]. Furthermore, the distribution of reinforcement particles in micro- and nano-composites is effectively enhanced by MA [1, 13–16]. To investigate the evolution of MMCs, NiTi was chosen as a model metal matrix system in the present work. It is well known that Ni, Ti, and their alloys have a great interest for wide applications owing to their excellent properties. Particularly, Ni and Ti alloy products prepared by powder metallurgy exhibit enhanced properties over those prepared by the conventional cast and wrought alloy products. Additionally, Ni-based alloys, particularly in superalloy form, demonstrate their effectiveness in challenging environments [17]. Recently, the reinforcement of Ni and Ti and their alloys with ceramics (e.g., Al2O3) or metals (e.g., Si) has attracted increasing interest. Al_2O_3 ceramic has been widely used in contact with metals for applications such as joining, sealing, and metal matrix composites. Since metal/Al_2O_3 composites possess high bond strength and excellent properties, they are desirable in many applications [18, 19]. The present work focuses on the preparation of 50Ni-50Ti, 45Ni-45Ti-10Si, and 45Ni-45Ti-10Al_2O_3 nanocomposite powders by mechanical alloying. Moreover, the effects of sintering temperature and the addition of Si or alumina on sinterability and mechanical properties (i.e., wear and friction) were investigated to obtain composites with appropriate mechanical properties useful for many industrial sectors and compatible with commercial standards.

2. Materials and Methods

In this work, ultra-pure Ti, Ni, Si, and Al_2O_3 powders were provided by Dop Organic Chemical Ind Ltd, Turkey. The purity, particle size, and particle shape of these powders are illustrated in Table 1 as provided by the supplier. Three alloy/composite batches were designed using the aforementioned materials; these were 50Ni-50Ti, 45Ni-45Ti-10Si, and 45Ni-45Ti-10Al_2O_3 in mass percentages. The designed symbols of these composites were A, B, and C, respectively. Nano powders were synthesized by milling the powder mixtures for 10 h in a planetary ball mill (model SFM-1 Desk-Top). The milling conditions were a ball-to-powder mass ratio (BPR) of 20:1, a ball diameter of 10 mm, and a rotation speed of 450 rpm. Stearic acid (0.1 wt%) was added as a process control agent to suppress excessive welding in the milling vial. To minimize sample overheating, the milling process was conducted with 2 h rest intervals every 2 h. The phase composition of the milled nanoparticles was qualitatively analyzed by X-ray diffraction (XRD) using a Philips PW 137 diffractometer with Ni-filtered Cu Kα radiation. The morphology and particle size were examined by transmission electron microscopy (TEM) using a JEOL JEM-1230 instrument. The milled powders were subsequently consolidated into 8 mm diameter by 4 mm length pellets using a hydraulic press. (Matest, C055D Digitec with maximum load 2000 kN) at 500 MPa. The pressed specimens were sintered in argon atmosphere (with oxygen impurities) at 1050, 1100, and 1200°C for 3 h with a heating rate of 10°C/min. The microstructure of some sintered samples was investigated

by scanning electron microscopy (SEM) "type Philips XL30". The mechanical wearing measurements (wear and friction coefficient) of sintered specimens were determined in an air atmosphere at room temperature with humidity of 35-40% using an oscillating ball-on-disk type tribometer wear tester. The wear measurements were performed according to the ASTM G-133-10 standard test method (linearly reciprocating ball-on-flat sliding wear). In this test, an alumina (Al_2O_3) ball with a 6 mm diameter is moving with a mean sliding speed of 2 mm/s and a normal load of 2 N. During the wear measurements, the friction coefficient was continuously measured by using a force sensor. The oscillating ball on-disk type tribometer wear tester is accredited according to ISO/IEC 17025:2005 requirements. Water contact angle measurement was used to determine the hydrophilicity of the treated surface at room temperature using a Phoenix 300 (Contact Angle Analyzer manufactured by S.E.O Co. Ltd.). The Phoenix 300 used a precision camera and advanced PC technology to capture the static droplet image and calculate the contact angle using the Sessile Drop method.

Table 1. Purity, particle size, and particle shape of starting powders.

Metal powder	Purity (%)	Mesh size (Mesh)	Particle size (μm)	Particle shape
Ni	99.9	100-200	50	Spherical
Ti	99.8	100-200	20	Flake
Si	99.9	100-200	20	Spherical
Al_2O_3	99.8	100-200	20	Spherical

3. Results and Discussion

3.1. Phase composition of milled powders.

It is worth mentioning that the original Ni and Si metal powders have cubic crystal structures, while Ti has a hexagonal close-packed structure [20-22]. On the other hand, α-Al_2O_3 powder has a rhombohedral crystal structure [23,24]. XRD patterns of milled 50Ni-50Ti, 45Ni-45Ti-10Si, and 45Ni-45Ti-10Al_2O_3 nano powder-mixtures milled for 10 h are shown in Figure 1. In these patterns, all peaks of Ni. Ti, Si, and Al_2O_3 also appeared in the patterns without formation of intermetallic phases [23, 24]. It is also indicated that there is an obvious shift in the position of the peaks. The dissolution of atoms related to minor matrix alloying elements or Al_2O_3 particles in the lattice during high-energy ball milling is the reason for this measurable shift. Furthermore, most of the peaks are broad and low in intensity owing to the refinement of the crystallite size and the enhancement of lattice strain [25]. The peak intensities of both Ni and Ti decrease after the addition of either Si or Al_2O_3. This is due to particle refinement.

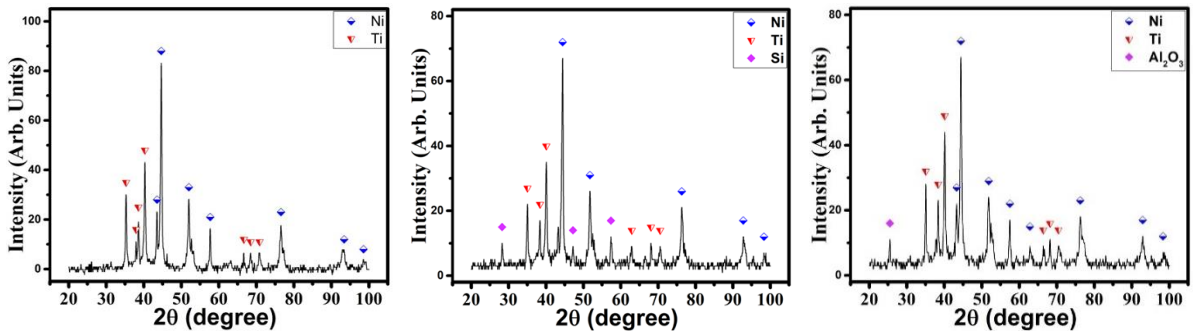

Figure 1. XRD patterns of powder mixtures **(A, B, C)** milled for 10 h.

3.2. Particle sizes and morphology of milled powders.

It is well known that, during mechanical milling, ductile metal particles deform while brittle ceramic particles fragment. After milling, the metal particles wet and coat the surfaces of the ceramic particles. Figure 2 shows TEM images of milled 50Ni-50Ti, 45Ni-45Ti-10Si, and 45Ni-45Ti-10Al_2O_3 nano powder-mixtures milled for 10 h. The figure shows that the particle sizes of the powder mixtures decrease after milling, compared to the original sizes of the supplied powders. The particle size of 50Ni-50Ti powder is remarkably decreased and reached about 85-350 nm after milling for 10 h. After adding Si and Al2O3 and milling for 10 h, the particle sizes were 104 and 28 nm, respectively. Good homogeneity in particle morphology and particle size appears after milling for 10 h. 50Ti-50Ni milled powder exhibits tough particle shape, while the powder mixtures 45Ni-45Ti-10Si and 45Ni-45Ti-10Al_2O_3 exhibit spherical particles. Plastic deformation, cold-welding, and fracture are the core steps that happen through mechanical milling and are responsible for particle morphology. The cold-welding of ductile metals causes an increase in the particle size, while the fracture tends to reduce the particle size [26]. As shown in Figure 2, the particles are agglomerated and welded, forming coarse particles in the 50NI-50Ti powder. After the addition of Si or alumina, particle sizes decrease and tend to form spherical particles. During the early stages of milling, ductile particles primarily experience plastic deformation, whereas brittle particles tend to fracture. Then, at the moment of ball collision, the ductile particles start to weld together, while brittle particles fit in between them. The starting powders are continually intermixed, leading to a homogeneous material with a uniform second-phase dispersion owing to the higher ball-mill velocity and particle collisions, which enhance powder refinement through deformation, welding, and fracturing. Since Al_2O_3 particles have higher hardness, they can also be used as milling media, which helps decrease particle size [27]. When welding and fracturing are repeated and reach a maximum (at equilibrium), a large number of new particle surfaces is created; no change occurs [27].

3.3. Phase composition and physical properties of sintered bodies.

It has been reported elsewhere [28] that the bodies (A, B, and C) sintered at different temperatures (i.e., at 1050, 1100, and 1200°C) were composed of different phases. For batch A (50Ni-50Ti) sintered at 1050°C, it is composed mainly of rutile and NiTi alloy with a small amount of unreacted Ni and Ti. At 1050°C, Ti is oxidized into rutile since it is a sensitive material for oxygen at high temperatures. During the penetration of oxygen, rutile is first formed on the outer layers, then inside the material. The presence of such oxide can enhance the mechanical performance of the composite [27]. When the temperature was increased to 1100°C, the amount of rutile was decreased while the quantities of Ni and Ti were increased, in addition to the presence of a small amount of Ni-Ti alloy and NiO. At 1100°C, the oxidation of Ti was low, so the amount of rutile was small too; at this temperature, the amounts of Ni and Ni were larger. It might be unreacted Ni or decomposed from the Ni-Ti alloy. At 1200°C, the quantities of formed phases were reduced, and the material seemed amorphous. Regarding the batch B (45Ni-45Ti-10Si) and C (45Ni-45Ti-10Al_2O_3), most of the phases were similar to those formed in the composite A, with the appearance of peaks for the phases of Si, Ti_2Si, NiTiSi, and Al_2O_3.

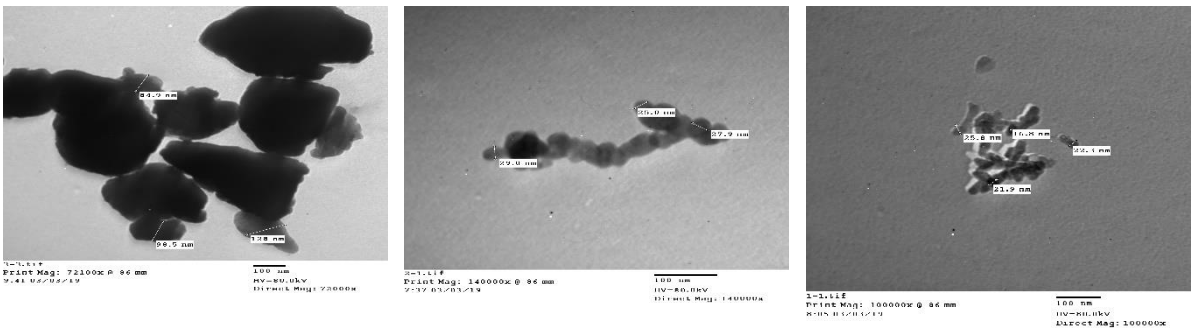

(a) **(b)** **(c)**

Figure 2. TEM images of powders **(A, B, C)** milled for 10 h.

Regarding the bulk density, relative density, and apparent porosity of A, B, and C composites sintered at 1050, 1100, and 1200°C for 3 h, it has been reported that the bulk density and relative density of sintered A, B, and C composites were increased with the firing temperature. Also, their values increased after the addition of silicon, decreased slightly after the addition of alumina, and remained higher than those of the NiTi alloy without additives (batch A). In all cases, the trends of apparent porosity were opposite to those of density. The maximum relative density was 91.2% and the minimum apparent porosity was 7.97%; both were obtained for composite B (45NI-45Ti-10Si).

The increase in relative density and the reduction in apparent porosity of sintered composites with rising sintering temperature are related to the higher diffusion rate and thermal activation of the grains, which lead to grain-grain interaction and the formation of surface-contacted grains [28,29]. Furthermore, some locked pores and grain growth are observed, leading to a homogeneous, dense microstructure [30,31]. On the other hand, the addition of Si and Al_2O_3, as well as the preparation of nano-scale starting powders, enhances the physical properties. The preparation of starting powders at the nanoscale increases surface area and consequently improves the physical and mechanical properties of sintered composites compared to those prepared from micro-sized powders [4]. Moreover, the addition of Si and Al_2O_3 as reinforcement particles has a direct effect on diffusion and contact between Ni-Ti matrix particles, contact-surface growth, the formation of closed pores, and grain growth. Therefore, the presence of Si or Al_2O_3 enhances the physical properties of sintered composites [30-31].

3.4. Microstructure sintered composites.

Figure 3 shows SEM images (different magnifications) of A, B, and C composites sintered for 3 h at 1200°C in an argon atmosphere. It is well known that the arrangement of particles and grains in microstructure begins during the pressing of starting powders owing to the mechanical interlocking of the particles [32] in the presence of higher grain boundaries. After sintering, new phases might be formed, grain-grain interaction or diffusion, close or open pore formation, and grain growth or grain reduction. As shown in Figure 3, a homogeneous, denser microstructure is observed, and the reinforcements are distributed homogeneously in the matrix. Some edge-plate-like grains are detected in the composite B (45Ni-45Ti-10Si); these grains seem to be related to silicon. These grains are interlocked in the matrix and close the pores. It is well known that the morphology of silicon (Si) grains in materials such as cast alloys and thin films can vary widely, including columnar, equiaxed, and plate-like structures. The shape and size of these grains are influenced by factors such as growth rate, temperature gradients, and the presence of impurities or grain refiners. Understanding these factors is

crucial for controlling the properties of materials, particularly in applications like semiconductors and metal alloys. The grain size of Si is larger than that of both the NiTi alloy and Al_2O_3. The composites that contain Si and Al_2O_3 (B and C) exhibit lower porosity than composite A.

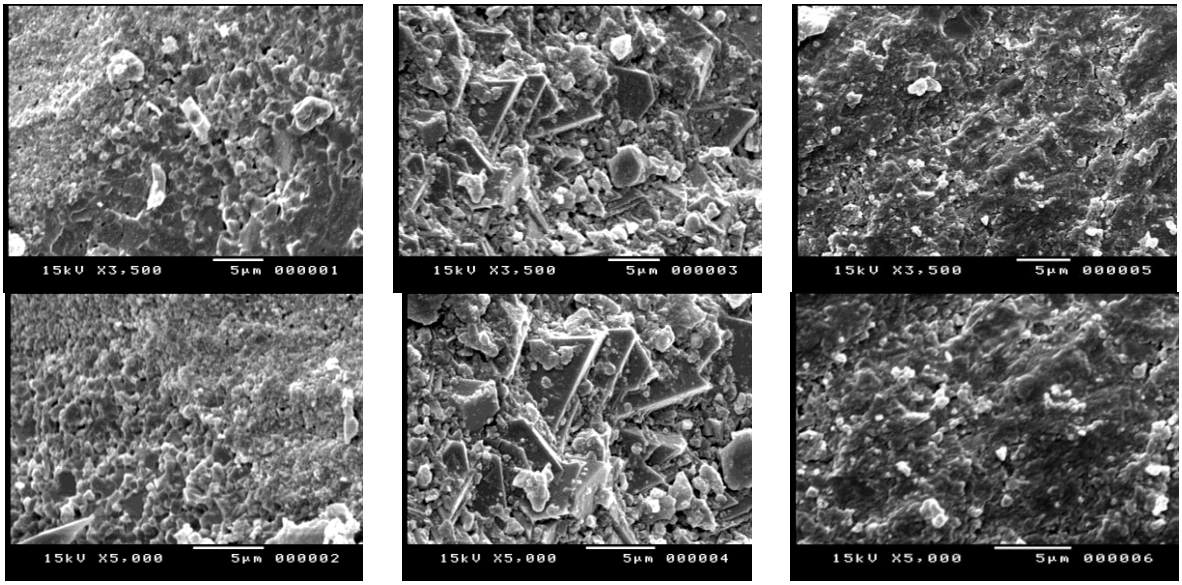

(A) **(B)** **(C)**

Figure 3. SEM images (different magnifications) of **(A, B, C)** composites sintered at 1200°C for 3h.

3.5. Wear and friction measurements of sintered composites.

The mechanical properties are typically influenced by the types of phases (matrix and reinforcement), porosity, grain refinement, and the uniformity of both the matrix and reinforcement [33, 34]. Namely, the improvement in mechanical properties can be explained as follows: first, the starting nanoscale powders facilitate the formation of sintered composites with fine grains and lower porosity after sintering at a suitable temperature [35, 36]. Secondly, the addition of reinforcements like Si or Al_2O_3 (hard ceramic particulate) can improve the mechanical properties. Si is an interesting alloying element for Ni-Ti (hard structures form) that increases the dislocation density of the Ni-Ti matrix, thereby enhancing the mechanical properties of the composite. On the other hand, alumina is a hard ceramic particle that can close pores and refine grains, as seen in the microstructure; in both cases, hard structures form after sintering [37-39].

Table 2 represents the values of wear rate and friction coefficient of A, B, and C composites sintered at different temperatures. The wear rate is the volume loss per unit meter per unit load (m^3/Nm). It is clear from Table 2 that the wear rate decreases for all composites with increasing sintering temperature and addition of Si or Al_2O_3. The decrease in wear rate with increasing sintering temperature is due to the formation of compact microstructures with lower porosity and higher density. Furthermore, the addition of Si and Al_2O_3 leads to a further decrease in porosity with the formation of hard phases in the case of composites B and C. The minimum wear rate ($11x10^{-6}$ mm^3/Nm) is obtained for the composite C, which contains alumina and is sintered at 1200°C. The existence/formation of hard ceramic or alloy phases leads to the enhancement of the load-bearing capacity of the composites. Also, these hard phases can form a more stable/resistant lubricating film on the tribolayer contact-surface of the composites. The formed hard tribolayer film reduces the amount of shear stress transmitted to the sliding material beneath the sliding contact area, leading to fewer plastic deformations in the subsurface region and lower wear rates in the composites. On the other hand, batch A

suffers heavy plastic deformation on the surface, which causes a higher wear rate of the alloy. From Table 2, it is also indicated that the friction coefficient decreases with increasing sintering temperature and addition of Si or Al_2O_3. The composite C, which contains alumina and is sintered at 1200°C, exhibits the best wear resistance (Wear rate =11x10-6 mm^3/Nm and friction coefficient 0.17). The presence of hard ceramic particles or the formation of a hard phase can transform the load on the composite and sliding surfaces, acting as solid lubricants, and then decrease the friction coefficient. Compared to the commercial materials, NiTi reinforced with Si or Al_2O_3 is very competitive. For example, compared with high-toughness SUS630 and CrMn white cast iron, NiTi alloy exhibits lower erosion wear loss and significantly greater resistance to erosion wear than 304 stainless steel [40-42].

Table 2. Friction coefficient and wear rates of A, B, and C composites sintered at different temperatures.

Composite	Sintering Temp, °C	Friction Coefficient	Wear Rate (x10^{-6} mm^3/Nm)
A	1050	0.75±0.2	41±1
	1100	0.72±0.2	33±1
	1200	0.65±0.2	31±1
B	1050	0.50±0.2	27±1
	1100	0.43±0.2	21±1
	1200	0.38±0.2	19±1
C	1050	0.30±0.2	20±1
	1100	0.21±0.2	18±1
	1200	0.17±0.2	11±1

3.6. Wetting behavior and water contact angle of sintered composites.

Ni-Ti alloy and its composites reinforced with ceramics or metals are widely used as biocompatible materials; therefore, the wetting behavior of these materials is of great importance in biomedical applications. Testing surface activity is the best way to evaluate surface quality in a wetting environment. One of the most important parameters affecting the wetting behavior of composites is the estimation of surface free energy [43]. The wettability of the prepared A, B, and C composites is evaluated using contact angle measurement. Decreasing the contact angle increases wettability and surface energy, while increasing the contact angle decreases wettability and surface energy [44]. Figures 4 and 5 show the water contact angles and surface energies, respectively, of the prepared A, B, and C composites sintered at different temperatures. The figures show that the contact angles of all composites are less than 90°, indicating a hydrophilic surface for all samples. The contact angle decreases with both increasing sintering temperature and the addition of Si or Al_2O_3. The contact angle decreases from nearly 82° for the composite A sintered at 1200°C to 41° for the composite C sintered at the same temperature.

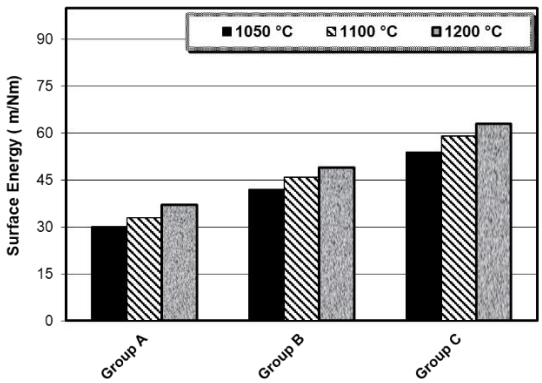

Figure 4. Surface energy of A, B, and C composites sintered at 1050, 1100, and 1200°C.

These hydrophilic surfaces with higher wettability are suitable for adhesion, spreading, and cell growth [45]. As shown in Fig.4, the surface energy of A, B, and C composites increases as the sintering temperature and addition of Si or Al_2O_3. It reaches 63 mN/m for the composite C sintered at 1200°C. Increasing the sintering temperature and adding Si or Al2O3 leads to the formation of harder phases, which enhance surface strengthening and, consequently, increase surface energy.

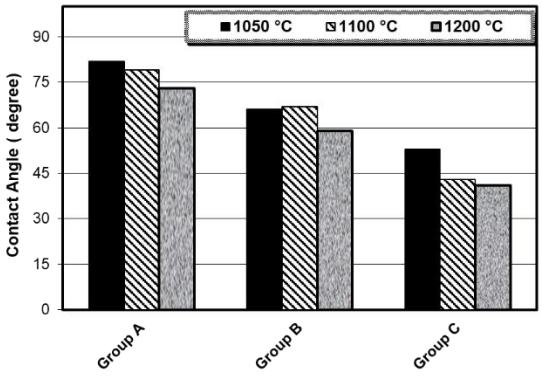

Figure 5. Contact angle of A, B, and C composites sintered at 1050, 1100, and 1200°C.

4. Conclusions

In this work, we succeeded in preparing 50Ti-50Ni, 45Ti-45Ni-10Si, and 45Ti-45Ni-10Al_2O_3 nano powders through the mechanical alloying method. Moreover, the prepared nanopoders were successfully utilized in the production of sintered composites after sintering at 1050, 1100, and 1200°C. The following are some concluding remarks of the work: after preparing the proposed powders, the Si and Al_2O_3 reinforcements were homogeneously dispersed within the NiTi matrix. Milling effectively reduced the particle size, resulting in average dimensions of 21 nm for the 50Ni50Ti nanocomposite, 27 nm for the 45Ni45Ti10Si nanocomposite, and 104 nm for the 45Ni45Ti10Al_2O_3 nanocomposite; increasing the sintering temperature and incorporating Si and Al_2O_3 improved wettability and increased surface energy. As a result, both the wear rate and the friction coefficient decreased; incorporating reinforcements and increasing the sintering temperature improved the mechanical properties. The best performance was obtained for the Al_2O_3-containing composite sintered at 1200°C (45Ni45Ti10Al_2O_3). For this composite, the wear rate and friction coefficient were 11×10^{-6} $mm^3/N \cdot m$ and 0.17, respectively.

Author Contributions

Conceptualization, M. Z.; methodology, H. A; validation, M. Z., H. A., and M. A.; formal analysis, M. Z. and H. A.; investigation, H. A, resources, M. Z., H. A., and M. A.; writing—original draft preparation, H. A.; writing—review and editing, M. Z.; supervision, I. H; All authors have read and agreed to the published version of the manuscript.

Institutional Review Board Statement

Not applicable.

Informed Consent Statement

Not applicable.

Data Availability Statement

Data supporting the findings of this study are available upon reasonable request from the corresponding author.

Funding

This research received no external funding.

Acknowledgments

Not applicable.

Conflicts of Interest

The authors declare no conflict of interest.

References

1. Muthukumaran, R.; Daniel, A.A.; Nithya, M.; Parthiban, A.; Sathish, T.; Giri, J.; Al-Lohedan, H.A. Characterization on properties of Al7050/TiC/BN hybrid metal matrix composite. *AIP Adv.* **2024**, *14*, 045318, https://doi.org/10.1063/5.0204280.
2. Taha, M.A.; Youness, R.A.; Zawrah, M.F. Review on nanocomposites fabricated by mechanical alloying. *nt. J. Miner. Metall. Mater.* **2019**, *26*, 1047-1058, https://doi.org/10.1007/s12613-019-1827-4.
3. Kumar, A. Microstructural Evaluation of Al-Al_2O_3 Composites Processed by Stir Casting Technique. *J. Mater. Eng.* **2024**, *2*, 267-272, https://doi.org/10.61552/JME.2024.04.004.
4. Channar, H.R.; Ullah, B.; Naseem, M.S.; Akhter, J.; Mehmood, A.; Aamir, M. Mechanical Properties and Microstructural Investigation of AA2024-T6 Reinforced with Al_2O_3 and SiC Metal Matrix Composites. *Eng* **2024**, *5*, 3023-3032, https://doi.org/10.3390/eng5040157.
5. Suri, J.; Shaw, L.L.; Zawrah, M.F. Synthesis of carbon-free Si_3N_4/SiC nanopowders using silica fume. *Ceram. Int.* **2011**, *37*, 3477-3487, https://doi.org/10.1016/j.ceramint.2011.06.003.
6. Lin, F.; Ren, M.; Wu, H.; Jia, F.; Yang, M.; Chen, Z.; Jiang, Z. In Situ Formation of Al_3Ti and Its Effects on the Microstructure, Hardness and Tribological Properties of Al Matrix Composites with Various Ti Contents. *Crystals* **2023**, *13*, 805, https://doi.org/10.3390/cryst13050805.
7. Zawrah, M.F; Aly, M.H. In situ formation of Al_2O_3–SiC–mullite from Al-matrix composites. *Ceram. Int.* **2006**, *32*, 21–28, https://doi.org/10.1016/j.ceramint.2004.12.005.
8. Warghat, S.; Sedani, C.; Rasane, A.; Maniyar, K.; Dhanwate, V.; Jadhav, S.P.; Deshmukh, S.; Gawande, J.; Biradar, R. An Extensive Study of Metal Matrix Composites and their Various Properties for Different Uses. *J. Mines Met. Fuels* **2024**, *72*, 949-955, https://doi.org/10.18311/jmmf/2024/45554.
9. Rahat, S.M.S.M.; Hasan, K.M.Z.; Mondol, M.M.H.; Mallik, A.K. A comprehensive review of carbon nanotube-based metal oxide nanocomposites for supercapacitors. *J. Energy Storage* **2023**, *73*, 108847, https://doi.org/10.1016/j.est.2023.108847.
10. Zhang, D.L.; Liang, J; Wu, J. Processing Ti_3Al–SiC nanocomposites using high energy mechanical milling. *Mater. Sci. Eng.* **2004**, *375-377*, 911–916, https://doi.org/10.1016/j.msea.2003.10.231.
11. Özbilen, S.; Vasquez, J.F.B.; Abbott, W.M.; Yin, S.; Morris, M.; Lupoi, R. Mechanical milling/alloying, characterization and phase formation prediction of $Al_{0.1–0.5}$(Mn)CoCrCuFeNi-HEA powder feedstocks for cold spray deposition processing. *J. Alloys Compd.* **2023**, *961*, 170854, https://doi.org/10.1016/j.jallcom.2023.170854.
12. Yang, W.; Dong, S.; Luo, P.; Yangli, A.; Liu, Q.; Xie, Z. Effect of Ni addition on the preparation of Al_2O_3–TiB_2 composites using high-energy ball milling. *J. Asian Ceram. Soc.* **2014**, *2*, 399-402, http://dx.doi.org/10.1016/j.jascer.2014.08.005.
13. Zebarjad, S.M.; Sajjadi, S.A. Microstructure evaluation of Al–Al_2O_3 composite produced by mechanical alloying method. *Mater. Des.* **2006**, *27*, 684–688, https://doi.org/10.1016/j.matdes.2004.12.011.
14. Ji, X.; Xiong, J.; Zhou, L. Microstructure Evolution and Mechanical Properties of Extruded AlSiCuFeMnYb Alloy. *Metals* **2024**, *14*, 774, https://doi.org/10.3390/met14070774.

15. Zhao, N.; Nash, P.; Yang, X. The effect of mechanical alloying on SiC distribution and the properties of 6061 aluminum composite. *J. Mater. Process. Technol.* **2005**, *170*, 586-592, https://doi.org/10.1016/j.jmatprotec.2005.06.037.
16. Vu, X.-T.; Nguyen, V.-H.; Tran, T.-V.; Nguyen, Q.-M.; Doan, D.-Q. Mechanical characteristics and deformation behavior of Al polycrystal reinforced with SiC particles. *J. Phys. Chem. Solids* **2023**, *183*, 111617, https://doi.org/10.1016/j.jpcs.2023.111617.
17. Zawrah, M.F.; Zayed, H.A.; Essawy, R.A.; Nassar, A.H.; Taha, M.A. Preparation by mechanical alloying, characterization and sintering of Cu–20wt.% Al_2O_3 nanocomposites. *Mater. Des. (1980-2015)* **2013**, *46*, 485-490, https://doi.org/10.1016/j.matdes.2012.10.032.
18. Xing, L.; Hao, S.; Huang, H.; Yao, L.; Ding, A.; Zhang, M.; Zhang, Y.; Zhao, X.; Wang, J.; Xu, R.; Liu, S.; Jiang, B. Ni-base superalloys enhanced by in-situ MC carbides precipitant on TiC nanoparticles. *Mater. Today Commun.* **2024**, *38*, 108262, https://doi.org/10.1016/j.mtcomm.2024.108262.
19. Suryanarayana, C.; Al-Aqeeli, N. Mechanically alloyed nanocomposites. *Prog. Mater. Sci.* **2013**, *58*, 383-502, https://doi.org/10.1016/j.pmatsci.2012.10.001.
20. Sajjadi, S.A.; Ezatpour, H.R.; Torabi Parizi, M. Comparison of microstructure and mechanical properties of A356 aluminum alloy/Al_2O_3 composites fabricated by stir and compo-casting processes. *Mater. Des.* **2012**, *34*, 106-111, https://doi.org/10.1016/j.matdes.2011.07.037.
21. Wyckoff, R.W.G. Second Edition. Interscience Publishers, New York Note: Cadmium Iodide Structure. *Crystal Structure* **1963**, *1*, 239-444.
22. Wu, H.; Hartman, M.R.; Udovic, T.J.; Rush, J.J.; Zhou, W.; Bowman Jr, R.C.; Vajo, J.J. Structure of the novel ternary hydrides Li_4Tt_2D (Tt= Si and Ge). *Acta Cryst.* **2007**, *63*, 63-68, https://doi.org/10.1107/S0108768106046465.
23. Taha, M.A.; Nassar, A.H.; Zawrah, M.F. In-situ formation of composite having hard outer layer based on aluminum dross reinforced by SiC and TiO_2. *Constr. Build. Mater.* **2020**, *248*, 118638, https://doi.org/10.1016/j.conbuildmat.2020.118638.
24. Zawrah M.F.; Schneider J; Zum Ghar, K.-H Microstructure and mechanical characteristics of laser-alloyed alumina ceramics, *Materials Science and Engineering* **2002**, *332*, 167 – 173, https://doi.org/10.1016/S0921-5093(01)01728-2.
25. Swanson, H.E. Standard X-ray diffraction powder patterns; US Department of Commerce, National Bureau of Standards: **1953**; Volume 25.
26. Jeyasimman, D.; Sivaprasad, K.; Sivasankaran, S.; Ponalagusamy, R.; Narayanasamy, R.; Iyer, V. Microstructural observation, consolidation and mechanical behaviour of AA 6061 nanocomposites reinforced by γ-Al_2O_3 nanoparticles. *Adv. Powder Technol.* **2015**, *26*, 139-148, https://doi.org/10.1016/j.apt.2014.08.016.
27. Zawrah, M.F.; Taha, M.A.; Abo Mostafa, H. In-situ formation of Al_2O_3/Al core-shell from waste material: Production of porous composite improved by graphene. *Ceram. Int.* **2018**, *44*, 10693-10699, https://doi.org/10.1016/j.ceramint.2018.03.101.
28. Taha, M.A.; Zawrah, M.F. Mechanical Alloying and Sintering of a Ni/10wt.%Al_2O_3 Nanocomposite and its Characterization. *Silicon* **2018**, *10*, 1351-1359, https://doi.org/10.1007/s12633-017-9611-4.
29. Zawrah, M.F.; Hassab-Allah, I.M.; Ata, M.H.; Shouib, H. Effect of Si, Al_2O_3, and aluminum dross on sinterability and properties of Ni–Ti metal matrix composites prepared by powder metallurgy. *Mater. Res. Express* **2019**, *6*, 096588, https://doi.org/10.1088/2053-1591/ab316e.
30. Zawrah, M.F.; Essawy, R.A.; Zayed, H.A.; Abdel Fattah, A.H.; Taha, M.A. Mechanical alloying, sintering and characterization of Al_2O_3–20wt%–Cu nanocomposite. *Ceram. Int.* **2014**, *40*, 31-38, https://doi.org/10.1016/j.ceramint.2013.05.099.
31. Wahsh, M.M.S.; Khattab, R.M.; Zawrah, M.F. Sintering and technological properties of alumina/zirconia/nano-TiO_2 ceramic composites. *Mater. Res. Bull.* **2013**, *48*, 1411-1414, https://doi.org/10.1016/j.materresbull.2012.12.024.
32. Zawrah, M.F.; Shaw, L. Liquid-phase sintering of SiC in presence of CaO. *Ceram. Int.* **2004**, *30*, 721-725, https://doi.org/10.1016/j.ceramint.2003.07.017.
33. Zawrah, M.F.; Shehata, A.B.; Kishar, E.A.; Yamani, R.N. Synthesis, hydration and sintering of calcium aluminate nanopowder for advanced applications. *C. R. Chim.* **2011**, *14*, 611-618, https://doi.org/10.1016/j.crci.2010.11.004.
34. Ishizaki, K.; Komarneni, S.; Nanko, M. Porous Materials: Process technology and applications, 1st Edition; Springer US: Boston, MA, **1998**; https://doi.org/10.1007/978-1-4615-5811-8.

35. Alemu, W.Y.; Chen, P.-L.; Chen, J.-K. Core-rim microstructure formation and mechanical properties of TiB_2 ceramics with TiC, B_4C, Co, and Mo sintering aids. *Ceram. Int.* **2023**, *49*, 40689-40694, https://doi.org/10.1016/j.ceramint.2023.10.052.
36. Amadi, A.; Mohyaldinn, M.; Ridha, S.; Ola, V. Advancing engineering frontiers with NiTi shape memory alloys: A multifaceted review of properties, fabrication, and application potentials. *J. Alloys Compd.* **2024**, *976*, 173227, https://doi.org/10.1016/j.jallcom.2023.173227.
37. Geetha, M.; Singh, A.K.; Asokamani, R.; Gogia, A.K. Ti based biomaterials, the ultimate choice for orthopaedic implants – A review. *Prog. Mater. Sci.* **2009**, *54*, 397-425, https://doi.org/10.1016/j.pmatsci.2008.06.004.
38. Ninarello, D.; Passaretti, F.; Nespoli, A. Body temperature NiTi alloys: effect of the heat treatment on the functional thermo-mechanical properties. *J. Therm. Anal. Calorim.* **2023**, *148*, 10757-10775, https://doi.org/10.1007/s10973-023-12437-1.
39. Tokat Birgin, P.Ç.; Kaya, E. Tribological and mechanical performance evaluation of hybrid reinforced copper composites. *J. Sci. Rep. A* **2024**, 51-67, https://doi.org/10.59313/jsr-a.1446422.
40. Yan, Y.-F.; Kou, S.-Q.; Yang, H.-Y.; Shu, S.-L.; Qiu, F.; Jiang, Q.-C.; Zhang, L.-C. Ceramic particles reinforced copper matrix composites manufactured by advanced powder metallurgy: preparation, performance, and mechanisms. *Int. J. Extrem. Manuf.* **2023**, *5*, 032006, https://doi.org/10.1088/2631-7990/acdb0b.
41. Bedolla-Becerril, E.; Garcia-Guerra, J.; Lopez-Morelos, V.H.; Garcia-Renteria, M.A.; Falcon-Franco, L.A.; Martinez-Landeros, V.H.; García-Villarreal, S.; Flores-Villaseñor, S.E. Tribological Behaviour of Al-2024/TiC Metal Matrix Composites. *Coatings* **2023**, *13*, 77, https://doi.org/10.3390/coatings13010077.
42. Jain, S.; Mishra, R.S. Effect of Al_2O_3 nanoparticles on microstructure and mechanical properties of friction stir-welded dissimilar aluminum alloys AA7075-T6 and AA6061-T6. *Proceedings of the Institution of Mechanical Engineers, Part E: Journal of Process Mechanical Engineering* **2022**, *236*, 1511-152, https://doi.org/10.1177/09544089211065534.
43. Zhou, G.; Ding, H.; Zhang, Y.; Hui, D.; Liu, A. Fretting behavior of nano-AL_2O_3 reinforced copper-matrix composites prepared by coprecipitation. *Metalurgija* **2009**, *15*, 169-179.
44. Liu, Y.; Wang, Y.-X.; Yang, Q.; Wang, F. Chemical and Wetting Analysis of the Ni-Ti Coating on SiC Improved by a 2-Step Coating-Sintering Process. *Materials* **2020**, *13*, 5235, https://doi.org/10.3390/ma13225235.
45. El-Hossary, F.M.; Negm, N.Z.; Abd El-Rahman, A.M.; Raaif, M.; Abd Elmula, A.A. Properties of Titanium Oxynitride Prepared by RF Plasma. *Adv. Chem. Eng. Sci.* **2014**, *5*, 1-14, https://doi.org/10.4236/aces.2015.51001.

Publisher's Note & Disclaimer